Laser and Particle Beams (2001), *19*, 15–22. Printed in the USA.

Generation and application of ultrashort X-ray pulses

D. VON DER LINDE,[1] K. SOKOLOWSKI-TINTEN,[1] CH. BLOME,[1] C. DIETRICH,[1] P. ZHOU,[1]
A. TARASEVITCH,[1] A. CAVALLERI,[2] C.W. SIDERS,[2] C.P.J. BARTY,[2] J. SQUIER,[2]
K.R. WILSON,[2] I. USCHMANN,[3] AND E. FÖRSTER[3]

[1]Institut für Laser- und Plasmaphysik, Universität Essen, D-45117 Essen, Germany
[2]Department of Chemistry and Biochemistry, 2, University of California, San Diego, La Jolla, CA 92093-0339, USA
[3]Institut für Optik und Quantenelektronik, Friedrich-Schiller-Universität Jena, 07743 Jena, Germany

(RECEIVED 22 December 2000; ACCEPTED February 2001)

Abstract

Relatively small-scale laser-driven sources of short wavelength radiation covering a range from the extreme ultraviolet to the hard X-ray regime are now available. Because the duration of the X-ray pulses is comparable to, or shorter than the laser pulse width, it is possible to carry out X-ray measurements with picosecond or femtosecond time resolution.

1. INTRODUCTION

The rapid progress that has been made in the generation of intense femtosecond laser pulses during the past decade has provided new opportunities for producing short pulse, short wavelength radiation (Gibbon & Förster, 1996; Mourou *et al.*, 1998). Laser-driven radiation sources with picosecond or even femtosecond pulse widths and photon energies ranging from, say, 100 eV up to several megaelectronvolts are now becoming available. These ultrashort X-ray pulses offer a unique combination of spatial and temporal resolution and thus make it possible to carry out entirely new types of experiments. The X-ray spectrum spans the range of wavelengths required to resolve spatial structure on an atomic scale. Our present knowledge of the structure of matter is to a large extent due to the application of X-rays and X-ray spectroscopies such as X-ray diffraction, X-ray absorption, and X-ray photoelectron spectroscopy, to name only a few. On the other hand, the femtosecond time regime, roughly speaking 10^{-14} to 10^{-13} s, is the characteristic time scale on which changes of atomic configurations take place. Examples include changes of the atomic arrangement associated with molecular vibrations and lattice vibrations and configuration changes in the course of elementary chemical reactions or during structural phase transitions. Over the past two decades, many different types of extremely fast phenomena have been successfully studied by means of femtosecond time-resolved *optical* spectroscopy. The recent award of the Nobel Prize in chemistry to Ahmed Zewail for his pioneering work in femtochemistry highlights the success of ultrafast optical science (Zewail, 2000). The perspective opening up now with femtosecond X-ray pulses is the combination of atomic scale spatial and temporal resolution in order to reveal both the structure and the evolution of matter.

Address correspondence and reprint requests to: Dietrich von der Linde, Institut für Laser- und Plasmaphysik, Fachbereich Physik, Universität Essen, 45117 Essen, Germany. E-mail: phy600@uni-essen.de

2. LASER-DRIVEN SOURCES OF SHORT PULSE, SHORT WAVELENGTH RADIATION

The success in using lasers to produce short wavelength radiation is basically due to the strong electromagnetic fields associated with ultraintense laser pulses. The optical electric field can be comparable to, or even larger than the Coulomb fields experienced by the electrons from the atomic nuclei. During the interaction with the laser field, electrons can pick up a kinetic energy of many thousands of electron volts, and this energy can be converted into short wavelength electromagnetic radiation by different interaction processes. At the present time there are two schemes that are the most promising for experimental application, at least in the foreseeable future. These are the generation of high-order harmonics in gases and X-ray emission from femtosecond laser-produced plasmas on solid surfaces.

2.1. High-order harmonic generation

The generation of optical harmonics of very high order has been studied extensively both in theory and experiment, particularly in noble gases (Krause, 1992; Corkum, 1993; Lewenstein *et al.*, 1994). In most of the earlier work, pulsed nozzles were used to produce a gas jet. Harmonic radiation was generated by focusing the fundamental laser radiation

https://doi.org/10.1017/S0263034601191020 Published online by Cambridge University Press

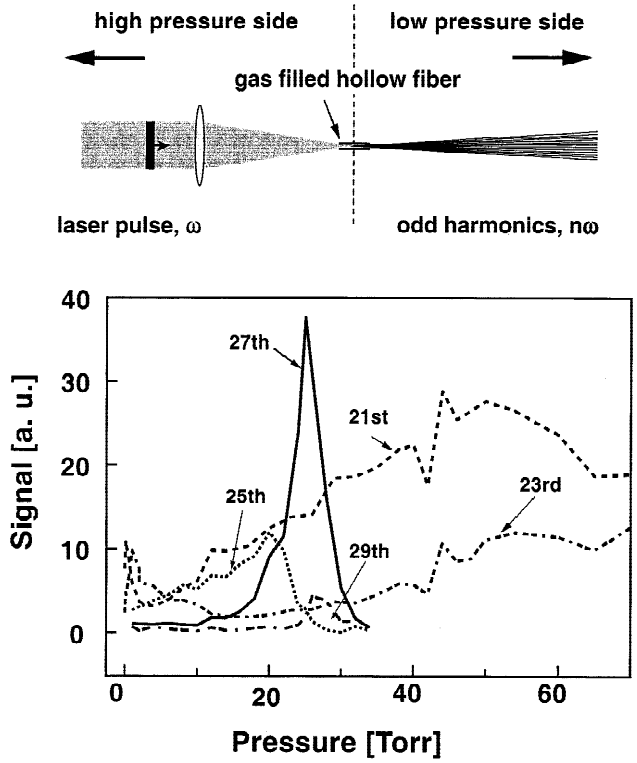

Fig. 1. Top: Schematic of high-order harmonic generation in gas-filled hollow fibers. Bottom: Harmonic generation in argon. Efficiency of the various harmonics as a function of gas pressure (high-pressure side of the fiber).

into the gas flow. More recently, harmonic generation in gas-filled hollow fibers has been demonstrated (Rundquist *et al.*, 1998; Schnürer *et al.*, 1998). From the point of view of applications, the hollow fiber scheme is very promising for a number of reasons. First, phase-matched harmonic generation over extended lengths of fiber is possible by judiciously balancing the dispersion of the fiber and the material dispersion of the partially ionized gas. Second, harmonic generation at high pulse repetition rates is much easier because pulsed nozzles, whose operation frequency is limited, are avoided. Third, gas consumption can be significantly reduced. The latter point represents a considerable advantage in experiments requiring ultrahigh vacuum conditions.

A simple schematic of a hollow fiber harmonic generator is depicted at the top of Figure 1. The device is housed in a tube of less than 10 cm length that can be directly flanged to an ultrahigh vacuum chamber. The bottom of Figure 1 shows the pressure dependence of a group of harmonics generated in an argon-filled piece of hollow fiber with an inner diameter of 167 μm and a length of 20 mm. The fundamental laser pulses were obtained from a CPA titanium sapphire laser at 1 kHz repetition rate. The pulse duration was $\approx$70 fs, and the energy at the entrance of the fiber was approximately 1 mJ.

Figure 2 shows the variation of the harmonic efficiency as a function of the backing pressure. For example, a distinct maximum of the 27th harmonic appears at 25 Torr. The observed behavior can be explained by the interplay be-

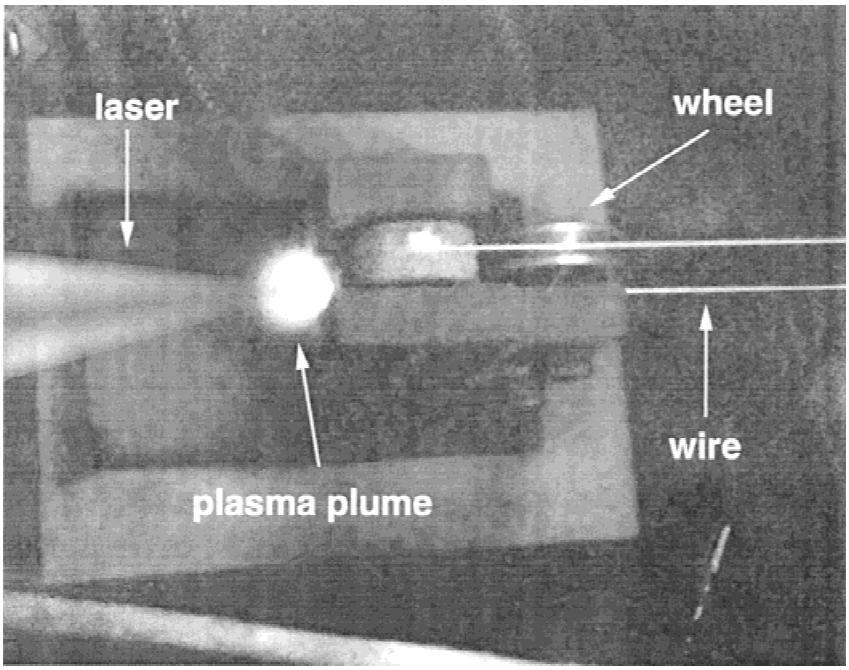

Fig. 2. The wire target used for X-ray generation. The lead cover that protects from exposure to hard X-rays is not shown.

https://doi.org/10.1017/S0263034601191020 Published online by Cambridge University Press

tween the pressure dependence of the phase mismatch and the absorption of the harmonic radiation in the gas.

Harmonic pulses with photon energies between 20 and 30 eV were used to perform time-resolved photoelectron spectroscopy of metals and semiconductors. The samples were photoexcited by the fundamental pulses, and the spectra of the photoelectron emission generated by the time-delayed harmonic probe pulses were measured with a time-of-flight (TOF) electron spectrometer. To avoid multiple photoelectron detection events in the TOF detector, the available harmonic intensity had to be reduced. Thus, the power of the generated harmonic was more than sufficient for this particular application. In these preliminary experiments, a grating had to be used to separate individual harmonics for the experiment. Because the group velocity dispersion of the grating leads to substantial temporal broadening of the harmonic pulses, the time resolution was limited to several picoseconds. The problem can be avoided by using XUV multilayer mirrors for selecting the desired harmonic frequency.

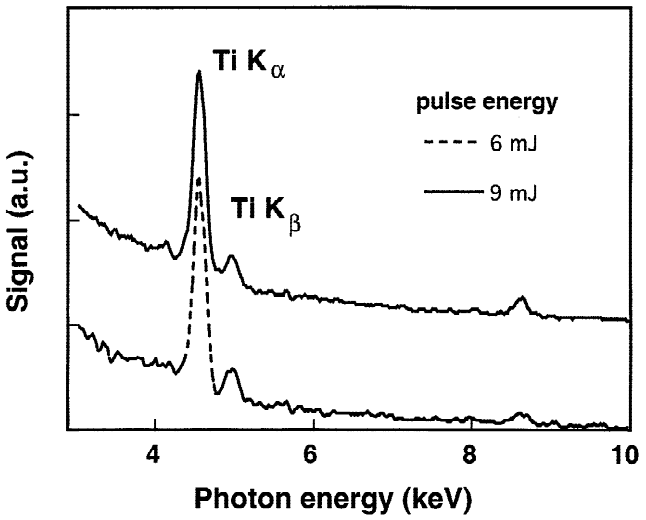

Fig. 3. X-ray spectra for two different laser energies, as obtained from a pulse-height analysis of the CCD camera output.

2.2. Laser–plasma source of kilovolt X rays

X-ray emission from laser-produced plasmas has been well known for a long time. However, the use of *femtosecond* laser pulses for plasma generation has opened up a wealth of interesting new possibilities and applications.

When an intense femtosecond laser pulse is focused onto the surface of solid material, a short-lived microplasma of high density and high electronic kinetic energy is generated. The microplasma represents a point-like source of short bursts of incoherent X rays (Rousse *et al.*, 1994; Jiang *et al.*, 1995). The typical spatial dimensions of the X-ray source are approximately 10 μm in diameter, and a few tens of nanometers in depth.

The X-ray spectrum consists of bremsstrahlung radiation and characteristic line emission, in particular relatively narrow K_α lines. The duration of the X-ray bursts is limited by the duration of plasma expansion and plasma cooling. Under suitable conditions, subpicosecond X-ray pulses can be expected (Reich *et al.*, 2000). However, measurements of the spatial dimensions and the time duration of the X-ray source are quite difficult. With a few exceptions, precise data are still lacking.

The commonly accepted explanation of the origin of the K_α emission (Rousse *et al.*, 1994; Bastiani *et al.*, 1997) assumes that the energetic electrons escape from the primary hot, highly ionized plasma and penetrate into underlying colder material. Here they knock out electrons from inner electronic shells of the atoms, producing core holes. Recombination with electrons from outer shells leads to characteristic line emission, very much as in an ordinary X-ray tube.

A common implementation of a laser–plasma X-ray source uses laser pulses focused onto a thin metallic wire (Rose-Petruck *et al.*, 1999). To avoid target erosion, the wire is continuously pulled across the focal plain, thus providing a fresh sample surface for each laser pulse. A photograph of our wire target is shown in Figure 2. An advantage of this type of X-ray source is that it can be continuously operated over hours simply by supplying a sufficiently large spool of wire.

A low-resolution X-ray spectrum of the titanium wire source is shown in Figure 3. The spectrum was obtained by analyzing the distribution of the pixel charges of a CCD chip exposed to the X rays from the titanium target. One can clearly distinguish the dominant titanium K_α line at 4.5 keV and the much weaker K_β line at 4.9 keV. The doublet structure of the K_α line due to spin-orbit splitting is not resolved.

If one wishes to use such an incoherent, pointlike X-ray source for experiments, an X-ray mirror with high reflectivity and large acceptance angle for efficient collection and focusing of X-ray photons is required. Excellent candidates are bent crystals, where one makes use of the strong Bragg reflection of X rays from lattice planes (Missalla *et al.*, 1999). Figure 4 shows a typical arrangement of a bent crystal in a Rowland geometry. We used a toroidally bent Si (311) platelet designed for one-to-one focusing of a titanium K_α radiation at 4.5 keV. The vertical and the horizontal radius of curvature must satisfy $Rv/Rh = \sin 2\Theta_B$, where Θ_B is the Bragg angle.

Experiments were carried out using laser pulses from a CPA titanium sapphire laser to drive the X-ray source. The laser system produced terawatt pulses of 120 fs duration at 10 Hz repetition rate. Figure 4 (bottom left) depicts the X-ray intensity distribution measured in the focal plane of the toroidal Si (311) mirror using an X-ray sensitive CCD camera. An approximately circular spot of about 80 μm in diameter was observed. The number of detected X-ray photons per pulse in the focal spot was approximately 10^4 for laser pulses of 30 mJ on the wire target.

https://doi.org/10.1017/S0263034601191020 Published online by Cambridge University Press

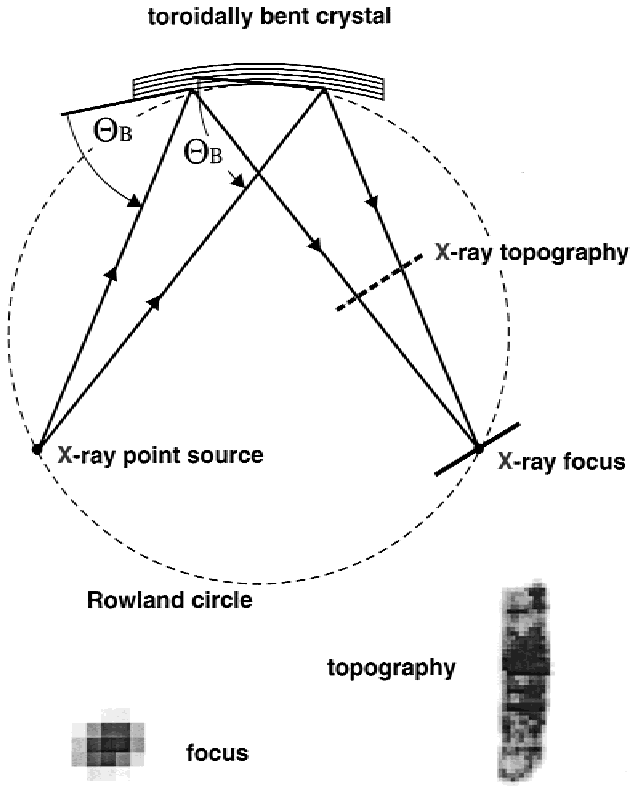

Fig. 4. Top: Focusing of an X-ray point source using a toroidally bent crystal (Rowland circle geometry). Bottom: X-ray distribution produced by a Ti-K_α wire source in the focal plain of a toroidal Si (311) mirror, as recorded with a CCD camera. The pixel size of the CCD detector is 27 μm.

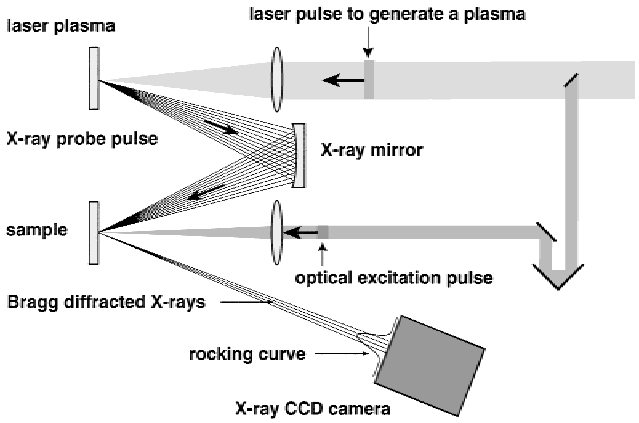

Fig. 5. Schematic of an optical pump/X-ray probe experiment for measuring time-resolved X-ray diffraction.

For efficient collection of the X rays emitted into the solid angle covered by the mirror, the Bragg condition must be satisfied over the complete surface area of the bent crystal. Figure 4 (bottom right) demonstrates that this is actually the case for our Si (311) mirror. The intensity distribution of the reflected X rays was measured in a plane close to the mirror, as indicated by the dashed line in Figure 4. The observed spatial distribution shown in Figure 4 (bottom right) reproduces the geometrical shape (4 mm by 15 mm) of the bent crystal rather well. Closer inspection indicates that with the exception of a relatively narrow border zone, the whole central part of the bent crystal is Bragg reflecting.

3. APPLICATIONS

Ultrafast time-resolved measurements in the X-ray regime can be performed using suitable variants of the pump-probe techniques which were established in time-resolved optical spectroscopy over the past three decades. Figure 5 illustrates the schematic of an optical pump/X-ray probe experimental setup for measuring ultrafast time-resolved X-ray diffraction, say from a single crystal. The basic laser pulse is divided into two beams with an adjustable time delay. The X-ray probe pulses are obtained from a microplasma generated by one of the beams, typically the more energetic one. A portion of the X rays is collected and focused onto the specimen under study by means of a suitable X-ray mirror. The optical pump pulse and the X-ray probe pulse must spatially overlap on the sample surface. The incident X-ray probe beam typically covers an angular range much larger than the angular width of the reflection characteristic of the crystal (*rocking curve*). The reflected X rays are detected by a CCD camera so that the complete rocking curves can be recorded.

Changes in the crystalline structure following the excitation by the pump pulse can be observed by recording the resulting changes of the rocking curve as a function of the delay time. The time resolution is determined by the duration of the X-ray pulses, which can be as short as a few hundred femtoseconds (Rischel *et al.*, 1997; Feurer *et al.*, 2001). We shall briefly discuss two recent experiments: (i) observation of a laser-induced transition from the crystalline to the liquid state, and (ii) the excitation and relaxation of coherent acoustic phonons.

3.1. Ultrafast phase transitions

There is extensive evidence that a transition from the solid to the liquid phase takes place on a time scale of a few hundred femtoseconds, when a semiconductor material like silicon is very strongly photoexcited by an ultrashort laser pulse (Sokolowski-Tinten *et al.*, 1995). The process was discovered in the early 1980s (Shank *et al.*, 1983*a*, 1983*b*) and attracted a lot of attention because the speed of the apparent phase transition could not be explained by normal thermal melting processes. Theory indicates that such an ultrafast structural transformation occurs in covalent semiconductors when an electron-hole concentration of approximately 10^{22} cm^{-3} is achieved, that is, when more than 10% of the covalent bonds are broken (Stampfli & Bennemann, 1990, 1992, 1994). Until very recently the only evidence for such ultrafast solid-to-liquid transitions

https://doi.org/10.1017/S0263034601191020 Published online by Cambridge University Press

were optical data (Saeta *et al.*, 1991; Sokolowski-Tinten *et al.*, 1995). Clearly, however, optical spectroscopy can provide only indirect information on the atomic structure.

As an example of the type of information available from optical measurements, time-resolved reflectivity spectra of silicon are depicted in Figure 6. These data show the evolution of the reflectivity after photoexcitation by an intense femtosecond pulse at 620 nm. They indicate a change from crystalline to metallic liquid reflectivity during a few hundred femtoseconds. Obviously, this type of extremely fast structural phase transition represents an ideal case to be studied by ultrafast X-ray diffraction.

Observation of the lattice structure by X-ray diffraction requires wavelengths shorter than the lattice constants, that is, a few Ångstroms or photon energies of several kilovolts. Generally speaking, X rays of this wavelength penetrate deeply into the crystal, typically much farther than the thickness of the molten surface layer that is produced by the laser pulse. This thickness is typically less than 100 nm. Under these conditions, X-ray diffraction would be strongly dominated by the bulk crystal. It would essentially ignore the very thin molten surface layer, unless special precautions were taken.

To overcome the problem, we have used thin crystalline layers of Ge, which were grown by surfactant-mediated heteroepitaxy on standard Si (111) wafers (Horn-von Hoegen, 1994). The key point is that one obtains a heterostructure with a highly perfect crystal layer whose lattice constant does not match the lattice constant of the substrate. In fact, the lattice mismatch is quite large in the Ge/Si (111) system, and the Bragg reflections from bulk Si and from the Ge surface layer are clearly separated (angular difference $\Delta\Theta \approx 1°$). This is demonstrated by Figure 7, which shows the camera read-out

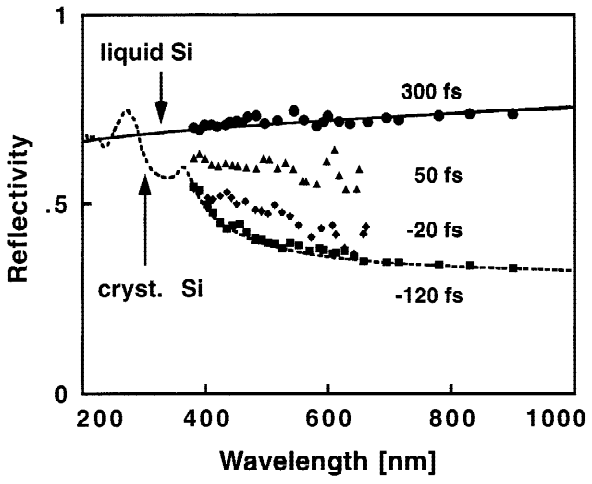

Fig. 6. Optical reflectivity spectra of femtosecond laser-excited silicon indicating an ultrafast structural phase transition from the solid to the liquid state. Solid line and dashed line: Reflectivity of liquid silicon and crystalline silicon, respectively. Symbols: Experimental results of time-resolved reflectivity measurements (Sokolowski-Tinten *et al.*, 1995).

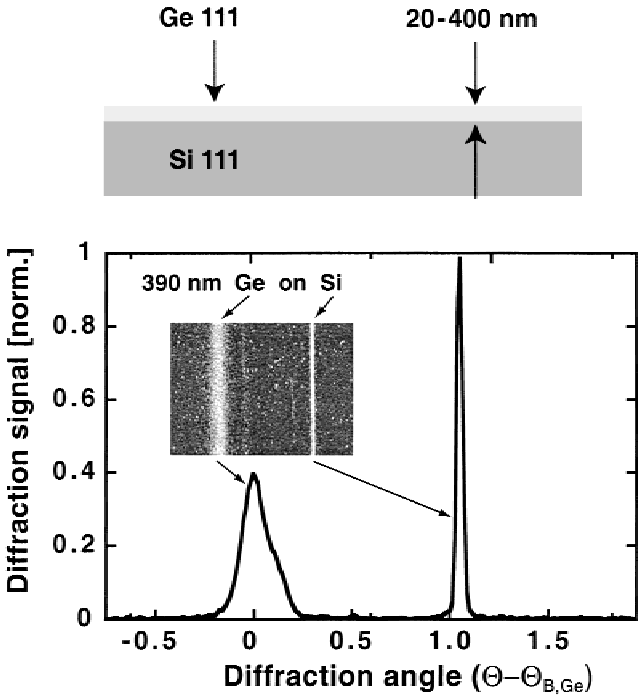

Fig. 7. Top: Outline of the Ge/Si heterostructure. Bottom: Rocking curve of the (111) Bragg diffraction from the Ge/Si-heterostructure. Insert: Portion of the actual image recorded with the CCD camera. Diffraction experiment performed with the Ti-K_α source and the Si (311) toroidal mirror.

of the (111) reflections from a 380 nm Ge/Si heterostructure. These data represent a 1-min recording with the X-ray pulses from a Ti-K_α source. The strong sharp line is due to the silicon substrate, whereas the broader and weaker peak represents the diffraction from the 380 nm germanium layer.

A time-resolved diffraction experiment was done under somewhat different conditions (Siders *et al.*, 1999). A Cu-K_α source at 8.05 keV was used without an X-ray mirror. The Ge/Si-heterostructure samples were photoexcited by the fundamental femtosecond pulses from a CPA titanium sapphire laser. The wafers were raster scanned to provide a fresh surface area for each laser pulse. Examples of (111)-Bragg-diffraction patterns measured at different delay times are depicted in the top part of Figure 8. The area between the two dashed lines in the diffraction patterns corresponds to the region of spatial overlap between the optical beam and the X-ray beam on the sample.

The curves in the lower part of Figure 8 show the measured change of the diffraction efficiency as a function of delay time between the laser excitation pulse and the X-ray pulse. It can be seen that in the center of the laser-excited area, the diffraction efficiency falls off to 70% of the undisturbed value in just a few picoseconds. A further decrease and a partial recovery of the diffraction are observed over several tens of picoseconds. It is interesting to note that at the border of the laser-excited area, at low laser fluence, the initial decrease of the diffraction is much slower than in the center at high fluence. Finally, a recovery of the diffraction

https://doi.org/10.1017/S0263034601191020 Published online by Cambridge University Press

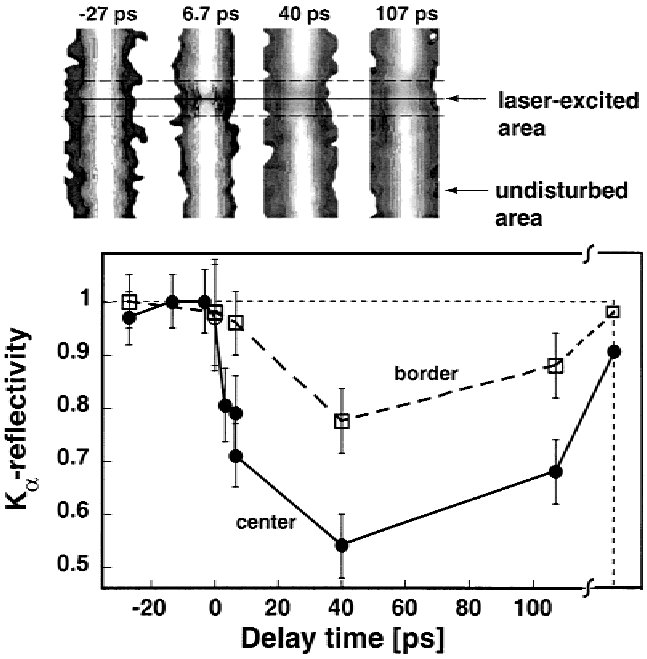

Fig. 8. Top: Four diffraction patterns from a Ge/Si-heterostructure at different delay times between the X-ray pulse and the laser excitation pulse. Bottom: Ge (111) X-ray diffraction signal from the laser-excited area of the heterostructure. Solid circles: High laser fluence in the center of the laser spot. Open squares: Low laser fluence at the border of the laser spot. Data measured with a Cu-K_α source at 8.05 keV (Siders *et al.*, 1999).

nearly to the original level is observed for very long delay times ("*infinity*").

Our time-resolved X-ray measurements reveal that a few picoseconds after the intense photoexcitation, the Ge lattice is destroyed, indicating an ultrafast structural change of the Ge crystal layer, in agreement with the earlier optical measurements. An angular shift resulting from a possible laser-induced lattice distortion can be ruled out as an explanation of the observed fast decrease of the Bragg diffraction, because in our experiment a sufficiently large angular range was simultaneously recorded.

The observed structural change is much too fast to be explained by an ordinary thermal melting process, even if strongly superheated conditions were assumed. If we take the sound velocity as an estimate of the ultimate upper limit of the propagation speed of the melt-front, it would take at least 20 ps to melt a 100 nm layer.

On the other hand, the observed slower melting rate at the border of the laser-excited area is also in excellent agreement with the previous experimental results. At lower local laser fluences, the critical carrier concentration for an ultrafast, electronically mediated transition is not reached. It has been demonstrated that under these conditions thermal melting takes place (Sokolowski-Tinten *et al.*, 1998). The slower further decrease of the diffraction in the center after the initial fast drop is presumably also due to thermal melting. It indicates melting of deeper layers of the Ge film, caused by the heat flow out of the initially molten top layer.

3.2. Ultrafast lattice dynamics

We have studied the damping of coherent acoustic lattice excitations following relaxation of thermal stress set up in the sample by short pulse laser excitation (Cavalleri *et al.*, 2000). As illustrated at the top of Figure 9, a femtosecond laser pulse (800 nm) is incident on the Ge/Si-heterostructure, preferentially depositing its energy in the Ge layer. After the thermalization of the optical energy, which takes several picoseconds, a uniform stress is set up in the layer. Release of the stress takes place by developing counterpropagating dilative strain waves from the surface and the Ge/Si interface, while a compressive strain wave is launched into the silicon substrate. The lower part of Figure 9 shows an example of the observed X-ray diffraction pattern from the Ge layer and bulk silicon, at a delay time of 100 ps after photoexcitation. In this experiment, the energy fluence of the laser pulses was well below the melting threshold. The doublet structure of the diffraction patterns is due to $K_{\alpha 1}/K_{\alpha 2}$ spin-orbit splitting of the *K*-shell emission from copper. The

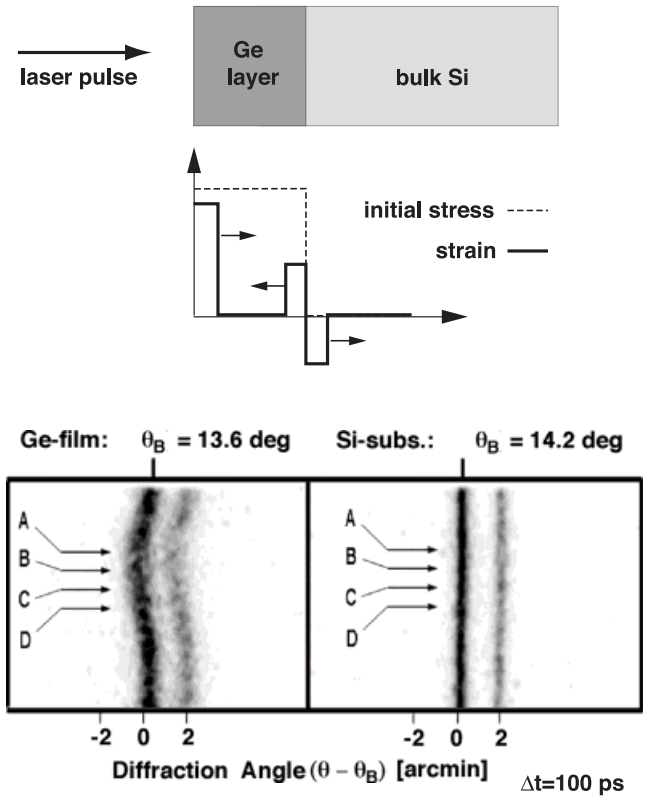

Fig. 9. Top: Outline of stress waves in the laser-excited heterostructure (below the threshold of the phase transition). Bottom: Example of diffraction patterns from the Ge layer and the silicon substrate at 100-ps delay time. The arrows A to D mark areas of different laser fluences.

https://doi.org/10.1017/S0263034601191020 Published online by Cambridge University Press

labels A to D mark the different local laser fluences on the sample surface, as determined by the beam profile of the laser excitation pulse.

The distinct shifts to lower angles of the Bragg diffraction from the Ge layer are quite apparent. The observed decrease of the diffraction angle indicates an expansion of the Ge layer. On the other hand, the much smaller positive angular shift of the silicon diffraction reveals the relatively weak compressive strain in silicon. Acoustic waves travelling towards the Ge/Si interface are partially reflected because there is a mismatch of the acoustic impedance of silicon and germanium. The reflection at the interface leads to strain waves bouncing back and forth between the surface and the interface. The round-trip time is given by $\Delta t = 2d/c_L$, where d and c_L are, respectively, the thickness of the Ge layer and the longitudinal sound velocity of germanium. With $d =$ 400 nm and $c_L = 5400$ m/s we obtain $\Delta t = 150$ ps.

Examples of results representing the dynamics of the acoustic waves excited by the laser pump pulse are shown in Figure 10. The data points represent the observed evolution of the Bragg diffraction angle from the Ge layer. At the lowest laser fluence corresponding to marker D in Figure 9, the variation of the diffraction angle looks like a damped oscillation. The measured oscillation period is ≈150 ps, in excellent agreement with the calculated round-trip time Δt. It might be expected that the damping of the acoustic waves in the Ge layer is due to the losses of acoustic energy to the substrate incurred upon each reflection at the interface. However, in this case the damping should be independent of the excitation fluence. The expected motion of the Bragg peak for this kind of damping model is represented by the solid lines in Figure 10: Only the losses to the substrate, but no intrinsic anharmonic or other damping processes are taken into account. It can be seen that this *harmonic model* gives a poor fit of the data. In particular, at high excitation fluence, the quantitative and qualitative disagreement is quite obvious.

The experimental data indicate a distinct increase of acoustic damping with laser fluence. We were able to explain this behavior by invoking anharmonic damping processes, including four-phonon collision processes. The corresponding decay rates increase with temperature, because the damping of the driven coherent modes involves interaction with thermal phonons. An excellent fit of the data for all fluences is achieved (dashed lines in Fig. 10) when these temperature dependent anharmonic damping effects are taken into account.

Although information on the damping of long wavelength acoustic phonons can also be obtained from other techniques, for example, acoustic absorption measurements or Brillouin scattering, we believe that these experiments represent the first step toward promising new applications of ultrashort X-ray pulses in lattice dynamics.

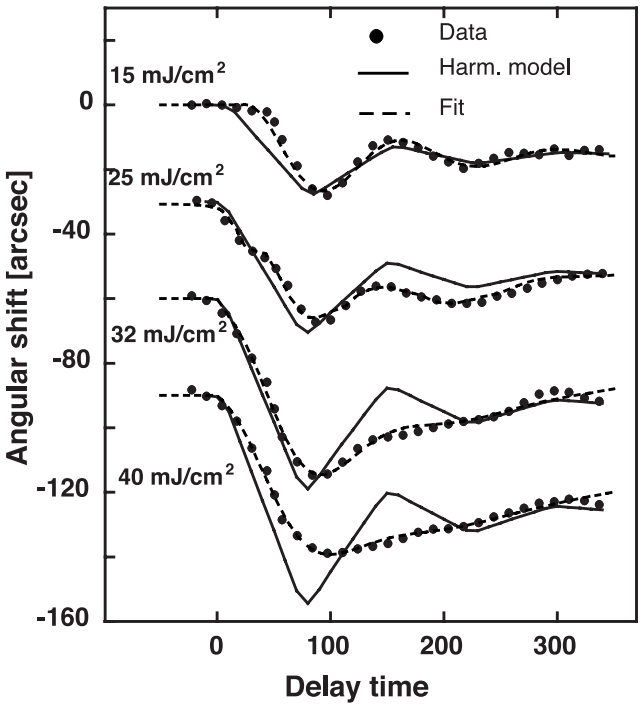

Fig. 10. Angular shift of the (111) diffraction pattern from the Ge layer as a function of delay time. Results for four different laser fluences are shown. Solid line: Only acoustic losses to the silicon substrate taken into account. Dashed line: Temperature-dependent anharmonic damping taken into account.

4. CONCLUSION

Laser-driven short pulse X-ray sources have matured to the point that time-resolved X-ray spectroscopy with picosecond and femtosecond resolution is possible. Certainly, only a few examples have been demonstrated as yet. We have shown that the new time-resolved X-ray techniques can reveal extremely fast structural transitions and the rapid dynamics of lattice distortions associated with acoustic perturbations. An attractive feature of laser-driven X-ray sources is that they enable relatively small-scale, almost table-top types of experiments. On the other hand, different large-scale facilities for the generation of powerful, short pulse X-ray sources are also available or will be in the future, for example free electron lasers and other schemes that make use of high-energy electron beams. At the present time, two highly developed disciplines of science are about to be tied together, X-ray science and ultrafast time-resolved spectroscopy. The combination of high time-resolution with atomic-scale spatial resolution should eventually enable researchers to record detailed, quasi-instantaneous pictures of complex atomic structures.

REFERENCES

Bastiani, S., Rousse, A., Geindre, J.P., Audebert, P., Quoix, C., Hamoniaux, G., Antonetti, A. & Gauthier, J.C. (1997). *Phys. Rev. E* **56**, 7179.

https://doi.org/10.1017/S0263034601191020 Published online by Cambridge University Press

Cavalleri, A., Siders, C.W., Brown, F.L.H., Leitner, D.M., Tóth, C., Squier, J.A., Barty, C.P.J., Wilson, K.R., Sokolowski-Tinten, K., Horn Von Hoegen, M., Von Der Linde, D. & Kammler, M. (2000). *Phys. Rev. Lett.* **85**, 86.

Corkum, P.B. (1993). *Phys. Rev. Lett.* **71**, 1994.

Feurer, T., Morak, A., Uschmann, I., Ziener, Ch., Schwoerer, H., Förster, E. & Sauerbrey, R. (2001). *Appl. Phys. B* **72**, 15–20.

Gibbon, P. & Förster, E. (1996). *Plasma Phys. Controlled Fusion* **38**, 769.

Horn-von Hoegen, M. (1994). *Appl. Phys. A* **59**, 503.

Jiang, Z., Kieffer, J.C., Matte, J.P., Chaker, M., Peyrusse, O., Gilles, D., Korn, G., Maksimchuk, A., Coe, S. & Mourou, G. (1995). *Phys. Plasmas* **2**, 1702.

Kieffer, J.C., Chaker, M., Matte, J.-P., Pepin H., Cote, C.-Y., Beaudoin, Y., Johnston, T.W., Chien, C.-Y., Coe, S., Mourou, G. & Peyrusse, O. (1993). *Phys. Fluids B* **5**, 2676.

Krause, J.L., Schafer, K.J. & Kulander, K.C. (1992). *Phys. Rev. Lett.* **68**, 3535.

Lewenstein, M., Balcou, Ph., Ivanov, M.Yu., L'Huillier, A. & Corkum, P.B. (1994). *Phys. Rev. A* **49**, 2117.

Missalla, T., Uschmann, I., Förster, E., Jenke, G. & Von Der Linde, D. (1999). *Rev. Sci. Instrum.* **70**, 1288.

Mourou, G.A., Barty, C.P.J. & Perry, M.D. (Jan. 1998). *Physics Today*, p. 22.

Reich, Ch., Gibbon, P., Uschmann, I. & Förster, E. (2000). *Phys. Rev. Lett.* **84**, 4846.

Rischel, C., Rousse, A., Uschmann, I., Albouy, P.A., Geindre, J.P., Audebert, P., Gauthier, J.C., Förster, E., Martin, J.L. & Antonetti, A. (1997). *Nature* (London) **390**, 490.

Rose-Petruck, C., Jimenez, R., Guo, T., Cavalleri, A., Siders, C.W., Ràski, F., Squier, J.A., Walker, B.C., Wilson, K. & Barty, C.P.J. (1999). *Nature* (London) **398**, 310.

Rousse, A., Audebert, P., Geindre, J.P., Fallios, F., Gauthier, J.C., Mysyrowicz, A., Grillon, G. & Antonetti, A. (1994). *Phys. Rev. E* **50**, 2200.

Rundquist, A., Durfee III, C.G., Chang, Z., Herne, C., Backus, S., Murnane, M. & Kapteyn, H.C. (1998). *Science* **280**, 1412.

Saeta, P., Wang, J.K., Siegal, Y.N., Bloembergen, N. & Mazur, E. (1991). *Phys. Rev. Lett.* **67**, 1023.

Schnürer, M., Cheng, Z., Sartania, S., Hentschel, M., Tempea, G., Brabec, T. & Krausz, F. (1998). *Appl. Phys. B* **67**, 263.

Siders, C.W., Cavalleri, A., Sokolowski-Tinten, K., Toth, C., Guo, T., Kammler, M., Horn Von Hoegen, M., Wilson, K.R., Von Der Linde, D. & Barty, C.P.J. (1999). *Science* **286**, 1340.

Shank, C.V., Yen, R. & Hirlimann, C. (1983*a*). *Phys. Rev. Lett.* **50**, 454.

Shank, C.V., Yen, R. & Hirlimann, C. (1983*b*). *Phys. Rev. Lett.* **51**, 900.

Sokolowski-Tinten, K., Bialkowski, J. & von der Linde, D. (1995). *Phys. Rev. B* **51**, 14186.

Sokolowski-Tinten, K., Bialkowski, J., Boing, M., Cavalleri, A. & von der Linde, D. (1998). *Phys. Rev. B* **5**, R18805.

Stampfli, P. & Bennemann, K.H. (1994). *Phys. Rev. B* **49**, 7299.

Stampfli, P. & Bennemann, K.H. (1992). *Phys. Rev. B* **46**, 10686.

Stampfli, P. & Bennemann, K.H. (1990). *Phys. Rev. B* **42**, 7163.

Zewail, A.H. (2000). *J. Phys. Chem. A* **104**, 5660.